Front. Optoelectron. China 2009, 2(1): 68–75
DOI 10.1007/s12200-008-0058-5

RESEARCH ARTICLE

Fabrication and characteristics of double-clad fiber Bragg gratings

Lijun LI (✉)[1,2], Wande FAN[2], Shenggui FU[2], Yange LIU[2], Shuzhong YUAN[2], Xiaoyi DONG[2]

1 College of Information and Electrical Engineering, Shandong University of Science and Technology, Qingdao 266510, China
2 Institute of Modern Optics, Nankai University, Tianjin 300071, China

Abstract A double-clad fiber Bragg grating (DCFBG) is a kind of grating which is directly written into the core of a double-clad fiber (DCF). Because of its special structure, DCFBGs have potential applications in fiber communication and sensing. In this paper, some of the recent studies on DCFBG are reviewed, and the photosensitivity and thermal decay of DCFBG fabricated in different DCFs are investigated. The DCFBGs of diversiform reflectivity are fabricated, and the maximum reflectivity of the grating is 99.9%. Finally, the special characteristics of DCFBG, such as nonlinear and stress, are illustrated.

Keywords double-clad fiber, fiber Bragg grating, photosensitivity, resonant nonlinearity

1 Introduction

Rare-earth-doped, cladding-pumped fiber lasers have been extensively studied in recent years [1–3] as important fiber-optic devices. Double-clad fiber (DCF) Bragg gratings are used for spectral filtering, wavelength tuning and sensing [4,5]. There are many methods to make fiber Bragg gratings (FBG), in which the phase-mask method makes the fabrication of FBG devices easier because there are less-stringent requirements on the ultraviolet (UV) source [6]. We can fabricate DCF Bragg gratings in high Germanosilicate host DCF or directly write the gratings into rare-earth-doped DCF [7]. However, since DCF is not a normal single-mode fiber, the study on the fabrication and the characteristics of the DCF Bragg gratings are thus important [8]. There are two main factors: the photosensitivity of the fiber, in which the grating is fabricated, and the thermal decay of the grating [9]. Because the DCF Bragg gratings are often fabricated in different inner-clad shape DCFs and used in high-power lasers, it is necessary to study the characteristics of DCF Bragg gratings, such as linear, nonlinear and stress characteristics [10,11].

A study on the fabrication and characteristics of double-clad fiber Bragg gratings has been carried out by our group in recent years [12–18]. This paper gives an overview of the progress of our work. In Sect. 2, the photosensitivity and the thermal decay of DCF Bragg gratings fabricated in different DCFs are investigated. The characteristics of DCF Bragg gratings are then shown in Sect. 3. Finally, conclusions are educed in Sect. 4.

Received January 2, 2008; accepted January 16, 2008

E-mail: nankaillj@163.com

2 Photosensitivity and thermal decay of DCF Bragg gratings (DCFBGs)

DCFs are hydrogen-loaded, and the phase-mask method is employed to write the DCFBG. The ultraviolet light source is a narrowband KrF excimer laser operated at 248 nm, the typical energy per pulse was 60 mJ, and the frequency of pulse is 25 Hz. The photosensitivity of the DCF is examined by studying the initial growth rate of the gratings fabricated into it. The Bragg wavelength shift is toward the longer wavelength side, which corresponds to an increase in the effective refractive index of the fiber core (Δn_{eff}). This can be determined by the equation

$$\Delta n_{\text{eff}} = \Delta\lambda/(2\gamma), \tag{1}$$

where $\Delta\lambda$ is the Bragg wavelength shift during the fabrication process of the grating and γ is the grating period. The shift of Bragg wavelength can be observed with the ultraviolet source exposed during the growth of the grating. The amplitude of the refractive-index modulation (Δn_{mod}) is estimated by using the following equation

$$\Delta n_{\text{mod}} = [\lambda/(\pi L n(V))]\tanh^{-1}(R)^{1/2}, \tag{2}$$

where L is the length of the grating, R is reflectivity and $n(V)$ is the overlap coefficient respectively.

The photosensitivity of Yb^{3+}-doped and normal DCF is studied experimentally. The variation of effective refractive index and amplitude of refractive-index modulation with the UV exposure time are observed. The diameter of the fiber core of Yb^{3+}-doped and normal DCF is 5 and 8 μm, respectively, and the diameter of the inner cladding is 125 μm. The grating length is 15 mm. We fabricate the grating with a phase-mask method, and the phase-mask period of Yb^{3+}-doped and normal DCF is 724.86 and 1073.3 nm, respectively. Gratings transmission spectra are measured with an Yb^{3+}-luminescence source and optical spectrum analyzer (OSA). Figures 1 and 2 show the evolution of the effective refractive index increment of the grating during the growth of the two FBGs, respectively.

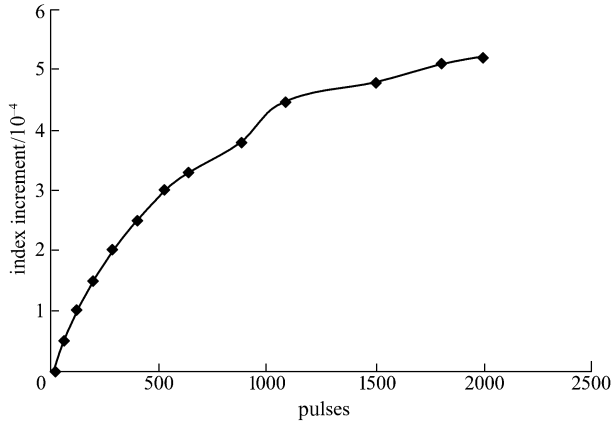

Fig. 1 Effective refractive index increment of grating during growth of Yb^{3+}-doped DCF Bragg grating

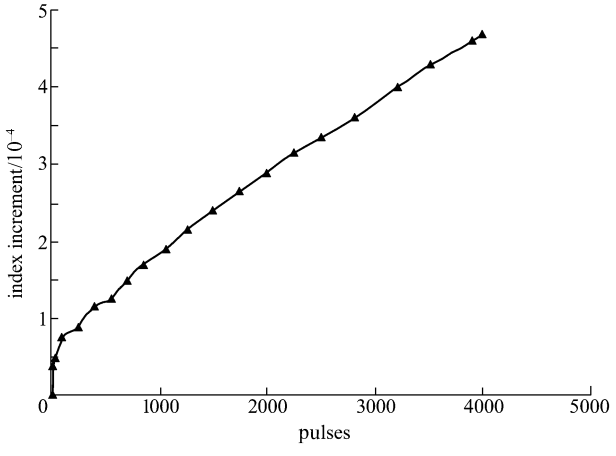

Fig. 2 Effective refractive index increment of grating during growth of normal DCF Bragg grating

From Figs. 1 and 2, it can be deduced that following UV exposure during the grating fabrication, the Bragg wavelength shift of Yb^{3+}-doped and normal DCF is observed to be 0.8 and 1 nm toward the longer wavelength, which corresponds to an increase in the effective refractive index of the fiber core of $\Delta n_{\text{eff}} = 5.188 \times 10^{-4}$ and $\Delta n_{\text{eff}} = 4.659 \times 10^{-4}$, respectively.

Figures 3 and 4 show the variation of refractivity of the grating with the UV exposure pulses, respectively, in which the typical energy per pulse is 50 mJ. From Eq. (2), the amplitude of refractive index modulation can be deduced from R. From Fig. 3, it can be found that the reflectivity of the Yb^{3+}-doped DCFBG increases sharply when the UV pulse number increases within 1000 pulses. When the pulse number is more than 1000, the increasing velocity of reflectivity becomes slow. The reflectivity achieves a maximum at 2000 pulses and the value is 99%.

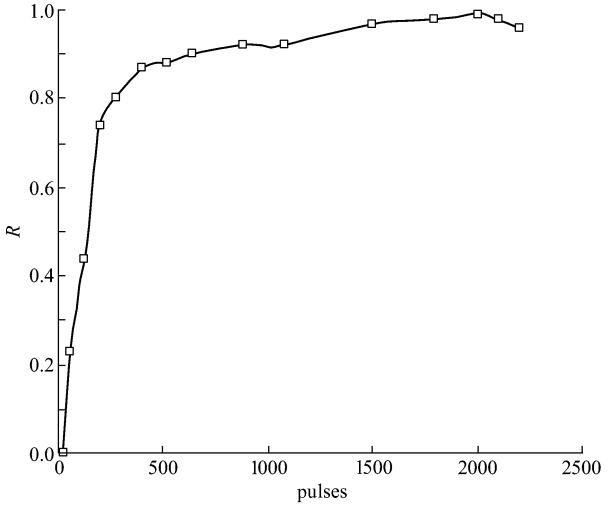

Fig. 3 Variation of reflectivity with UV exposure pulses of Yb^{3+}-doped DCF Bragg grating

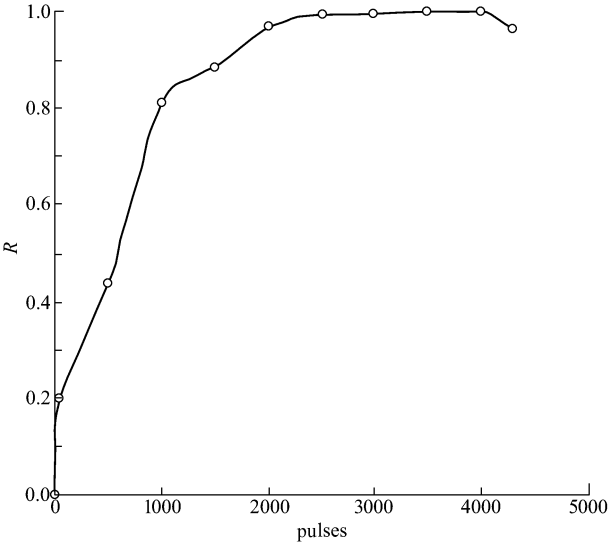

Fig. 4 Variation of reflectivity with UV exposure pulses of normal DCF Bragg grating

From Fig. 4, it can be found that the reflectivity of the normal DCFBG increases sharply when the UV pulse number increases within 2000 pulses. When the pulse number exceeds 2000, the increasing velocity of reflectivity becomes

slow. The reflectivity achieved the maximum at 4000 pulses and the value is 99.9%.

Figures 5 and 6 show the transmission spectra of the two FBGs. The reflectivity of gratings equals 99% for the Yb^{3+}-doped DCFBG and 99.9% for the normal DCFBG, respectively.

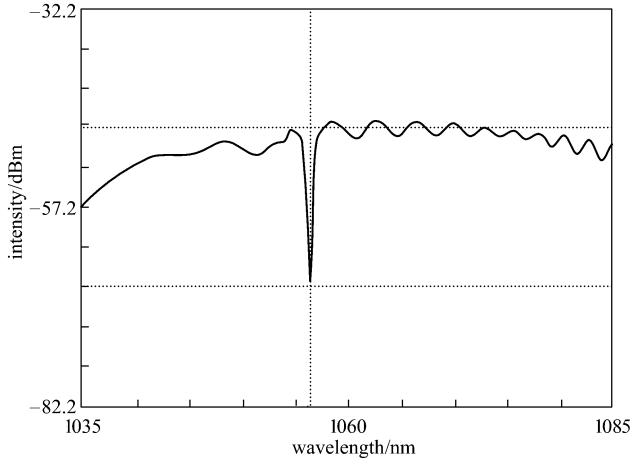

Fig. 5 Transmission spectrum of Yb^{3+}-doped DCF Bragg grating

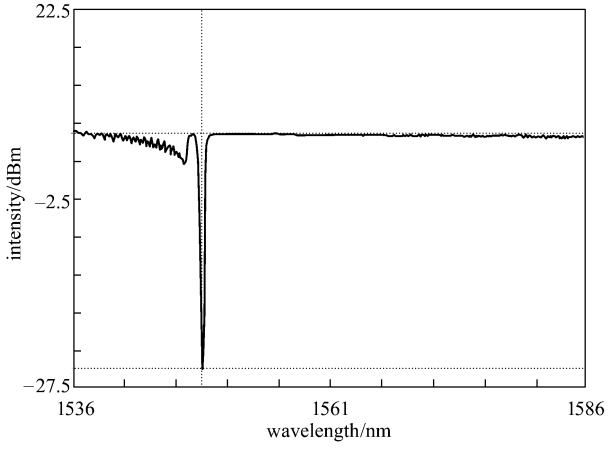

Fig. 6 Transmission spectrum of normal DCF Bragg grating

Bragg gratings are fabricated in Yb^{3+}-doped DCF. The thermal decay is investigated under the temperature of 100°C, 150°C, 200°C, and 250°C, respectively, and the gratings are maintained in an oven for 300 minutes at each of these temperatures. The gratings transmission spectrum is measured with a broadband source and OSA. Using the experimental data obtained, the thermal decay characteristics can be modeled. The experimental result is shown in Fig. 7, where R_0 is the reflectivity of the grating before being annealed. It is found that with the time prolonged, the reflectivity of the gratings declines. At the beginning of annealing, the reflectivity of the gratings declines sharply and become subtle in the intervening time.

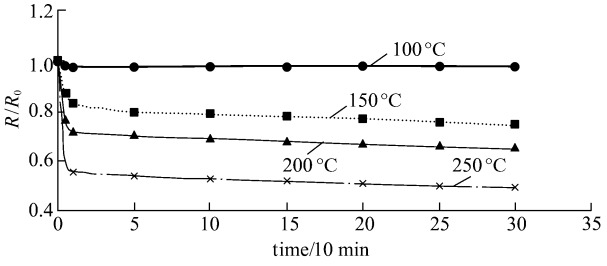

Fig. 7 Thermal decay of DCFBGs at various temperatures

3 Characteristics of DCFBGs

In a material with intensity-dependent refractive index, the refractive index n can be written as follows

$$n = n(I) = n + \Delta n(I,x,y,z), \tag{3}$$

where I is the intensity; and x, y and z define the position in the fiber. Nonlinearity due to the Kerr effect is described by the above equation with

$$\Delta n(I,x,y,z) = n_2 I(x,y,z), \tag{4}$$

where n_2 is the nonlinear parameter, which can be used to express the nonlinear intensity of the fiber.

The resonant nonlinearity effect in the fiber Bragg grating is that the refractive index of the signal-wave light changes through the variety of other wavelengths' light intensity. In rare-earth-doped fibers, the refractive index at a given wavelength is affected at relatively distant parts of the spectrum. By pumping the fiber at a suitable wavelength, resonant nonlinear processes can be produced. Taking the case of Yb^{3+}-doped DCF, the energy level structure consists of $^2F_{7/2}$-$^2F_{5/2}$ states corresponding to infrared absorption at 976 nm. Thus, the absorption of the pump light at 976 nm will result in an associated change in refractive index of the signal wavelength in the Yb^{3+}-doped DCF Bragg grating. The Bragg reflection wavelength is given by

$$\lambda_B = 2n_{eff}\gamma, \tag{5}$$

where λ_B is the Bragg wavelength, n_{eff} is the initial effective index, and γ is the grating pitch-width.

Using Eqs. (3), (4) and (5), n_2 can be calculated and given by

$$\Delta\lambda_B = 2\Delta n\gamma, \tag{6}$$

$$n_2 = \Delta n/I. \tag{7}$$

It is obvious that through the shift of the Bragg wavelength, resonant nonlinearity can be deduced when the pump power I changed.

In our experiment, we write the Bragg grating into the core of the Yb^{3+}-doped DCF. Figure 8 shows the transmis-

sion spectra of the grating, and the transmission dip appears at 1056 nm. To study the resonant nonlinearity effect in the DCFBG, we can take advantage of the special structure of DCF, in which the pumping light transmits in the first clad of the fiber. This grating as the output mirror of the laser is spliced to the same active DCF, and the laser configuration is shown in Fig. 9.

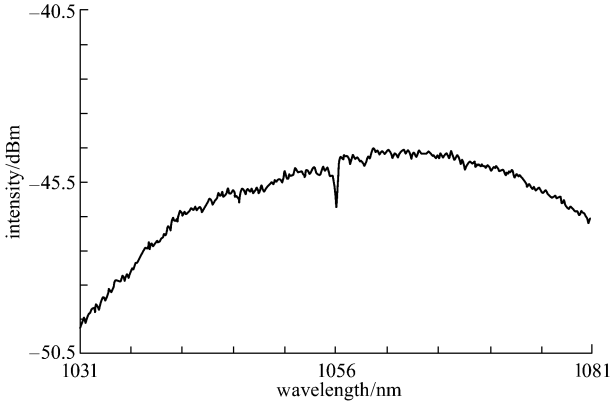

Fig. 8 Transmission spectrum of DCF Bragg grating

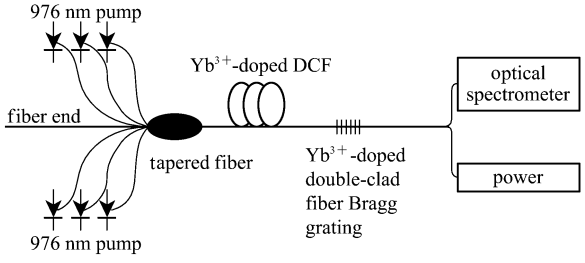

Fig. 9 Experimental set-up of DCF laser

The fiber in this F-P laser is a 20-meter-long Yb^{3+}-doped DCF. Its first circular cladding is undoped fused silica, and the diameter of outer round cladding is 125 μm. The fiber end is built as the fore-cavity mirror. The output mirror is a DCF Bragg grating whose reflectivity is nearly 30%. Six multimode 976 nm pump lasers pump the Yb^{3+}-doped DCF. The maximum power of every pump laser is nearly 1 W. A tapered fiber bundle is used to couple all pumps and the signal to the double-clad fiber. Figure 10 shows the spectrum of the laser. It can be seen from the figure that there is a mass of residual pump laser at the output end of the laser. Figure 11 shows the stability of the laser, while Fig. 12 illustrates the process of the laser wavelength shift with increasing pump power. The spectrum at the beginning of laser production is shown in Fig. 12(a). The central wavelength is 1056 nm, similar to the reflected central wavelength of the grating, and the pump power is 0.28 W at this time. The spectrum at this power is saved as the reference curve, then the output of the laser when the pump power is 0.56, 0.9, 1.22, 1.57 and 1.8 W is observed respectively. As the pump power is enhanced, the laser central wavelength shifts gradually to a longer wavelength. The process of the shift is shown in Figs. 12(b)–12(f). From these figures, it can be deduced that the Bragg wavelength of the grating shifts gradually to a longer wavelength with enhancing power of residual pump light. Figure 12(f) shows the laser wavelength, which is 1056.2 nm when the pump power reaches the maximum value. The maximum value, which is 1.8 W, can be found by measuring the power from the output end of the laser. Given the structural advantage of DCF and the constant environment temperature, the shift of the grating central wavelength does not result from the thermal effect in the fiber. Thus, we can say that this shift is the result of the resonant nonlinearity of the grating. By measuring the shift of the output wavelength, we can calculate the resonant nonlinearity of the double-clad fiber Bragg grating.

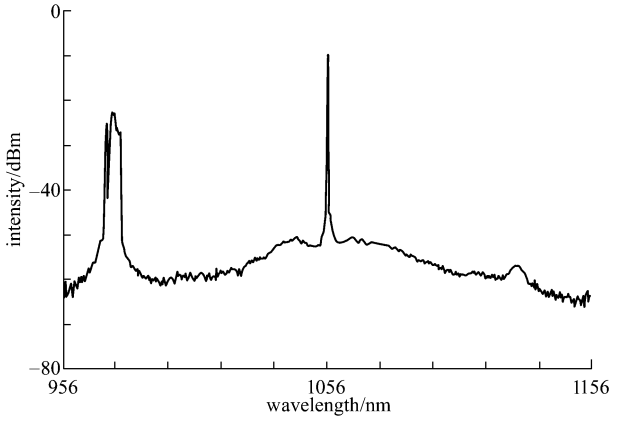

Fig. 10 Output spectrum of laser with residual pump light

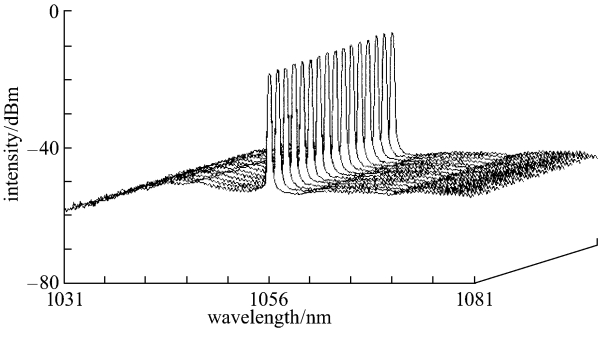

Fig. 11 Repeated scan of output spectra of laser

Double-clad fibers have different cladding structures, such as rectangular, star-shape and circular. They are all in use to provide efficient absorption of pump energy by the fiber core. This raises new questions about laser dynamics, stability, and polarization properties. In particular, the asymmetric structure of such fibers, typically with a rectangular inner cladding surrounding a circular core, prompted our investigation of the birefringence properties.

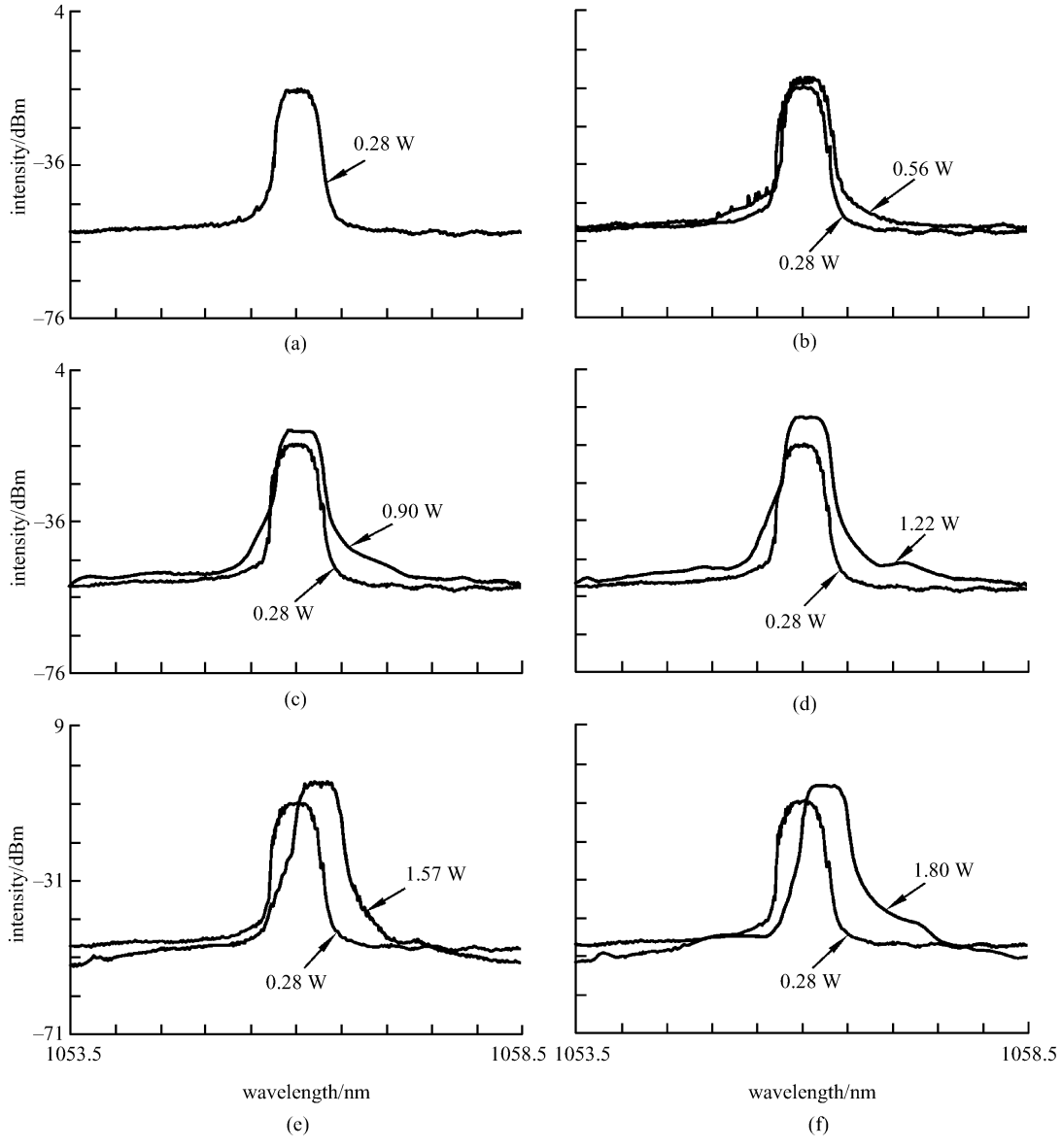

Fig. 12 Several output spectra over entire shifting range

Strain-induced birefringence in rectangular inner cladding Yb^{3+}-doped DCFBG is studied. The grating is directly fabricated in the rectangular inner cladding DCF with the phase-mask method, yielding reflectivity of ~30% and reflection peak wavelength of 1055.2 nm. The rectangular inner cladding DCF with elliptical cladding is studied. The slow and fast axes of the core coincide with those of the cladding. We apply stress on the DCFBG along the short axis of the inner cladding. The refractive index of the FBG changes and the FBG becomes birefringent. Two plane-polarized waves propagate in line with two directions: one is parallel and the other is perpendicular to the direction of the applied load. We assume that the principal optical axis aligns with x-, y-, and z-Cartesian axes. The induced birefringence B of the light propagating along the z-axis is given by

$$B = B_0 + \frac{|\Delta n_y - \Delta n_x|}{n_{\text{eff}}}, \tag{8}$$

where B_0 is the intrinsic birefringence induced by the elliptical inner cladding, n_{eff} is the initial core refractive index of the undisturbed optical fiber, and Δn_x and Δn_y are the refractive index changes due to the applied loads for the x and y polarizations respectively. The refractive index that changes due to the photo-elastic effect and develops into the first order are given by

$$\Delta\left(\frac{1}{n_m^2}\right) = p_{mn}\varepsilon_n,\ m,n = 1,2,3,..., \tag{9}$$

where p_{mn} is the photo-elastic coefficient, m and n are number of mode, and ε_n is the strain tensor, respectively.

The Bragg grating reflection wavelength is given by $\lambda = 2n_{\text{eff}}\gamma$. FBG wavelength shifts when the photo-elastic coefficient changes. Under the isothermal condition, the shift is given by

$$\mathrm{d}\lambda = \left[2\Lambda\left(\frac{\partial n_{\text{eff}}}{\partial P}\right) + 2n_{\text{eff}}\left(\frac{\partial \gamma}{\partial P}\right)\right]\mathrm{d}P. \qquad (10)$$

By calculating the core refractive index changes and the FBG periodicity deformation caused by the applied disturbance, the Bragg wavelength changes can be deduced.

With Eqs. (8)–(10), for x-polarization the Bragg wavelength shifts can be given by

$$\Delta\lambda_x = 2n_x\gamma\left[-\frac{n_x^2}{2}(p_{11}\varepsilon_x + p_{12}\varepsilon_y) + \left(1-\frac{n_x^2}{2}\right)p_{12}\varepsilon_z\right], \quad (11)$$

and for y-polarization it can be given by

$$\Delta\lambda_y = 2n_y\gamma\left[-\frac{n_y^2}{2}(p_{12}\varepsilon_x + p_{11}\varepsilon_y) + \left(1-\frac{n_y^2}{2}\right)p_{12}\varepsilon_z\right]. \quad (12)$$

It is obvious that the two wavelengths shift synchronously with axial strain ε_z, and wavelength space changes when lateral strains ε_x, ε_y are applied.

To detect the birefringence, we use this rectangular inner cladding DCF as active fiber and this grating as the output mirror of an Yb^{3+}-doped DCF laser. The diameter of the rectangular inner cladding is 100 μm × 85 μm. A polarization controller (PC) is inserted into the cavity, through which we can control the state of polarization of wave in the cavity. Figure 13 shows the spectrum of the grating without side stress.

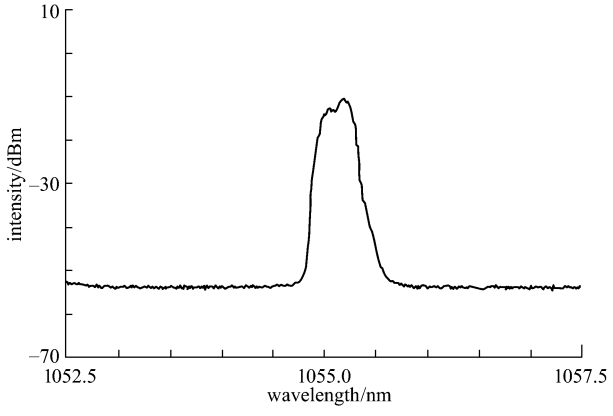

Fig. 13 Spectrum of grating without side stress

The strain applied device configuration is shown in Fig. 14. Strain is applied to the DCFBG by being located in the tuning frame, and the FBG is placed between two pieces of Perspex. FBG is applied lateral strain through a screw. An optical spectrum analyzer with resolution of 0.1 nm monitors the laser output spectra. When FBG is applied lateral strain, the FBG can become birefringent, therefore the reflection peak of the FBG becomes two peaks and the laser also has two wavelengths. The laser wavelength spacing can be tuned by the Perspex and screw. When screwed, the Perspex can apply a lateral strain to the FBG, which can produce birefringence in the fiber through the strain-optic effect. The stress in the fiber can be estimated by the screwed angle. The birefringence can be increased by applying the lateral strain in line with the slow axis, and with a corresponding increase in the wavelength spacing, two wavelengths will shift synchronously.

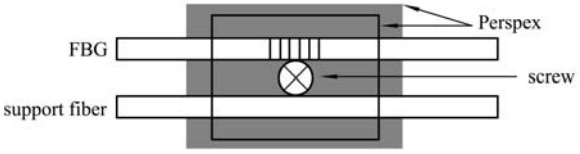

Fig. 14 Strain applied device configuration

Three kinds of lasing can be observed when the PC is adjusting. In the second state, only one polarization can oscillate, and these two states are orthogonal polarized to each other. Thus, only one wavelength can be observed. In the third state, the orthogonal linearly polarized modes coexist. Figure 15 shows the output spectrum of the laser with the screwed angle of 100°. Two wavelengths are 1056.4 and 1057.2 nm, respectively, and the side-mode suppressive ratio is about 29 dB. The laser outputs at room temperature are stable. Figure 16 shows the dependence of the wavelength spacing $\Delta\lambda$ on lateral strain, where linear responses are observed. The wavelength space can be tuned from 0 to 0.8 nm. Following these, Fig. 17 shows the dependence of Bragg reflection wavelength variation $\Delta\lambda_B$ on the screwed angle for two polarized directions, which can be tuned to 1.2 and 2.0 nm, respectively. When strain is applied, the Bragg reflection wavelength variation of one polarization is larger than the other because of the photoelastic property of the optical fiber's material.

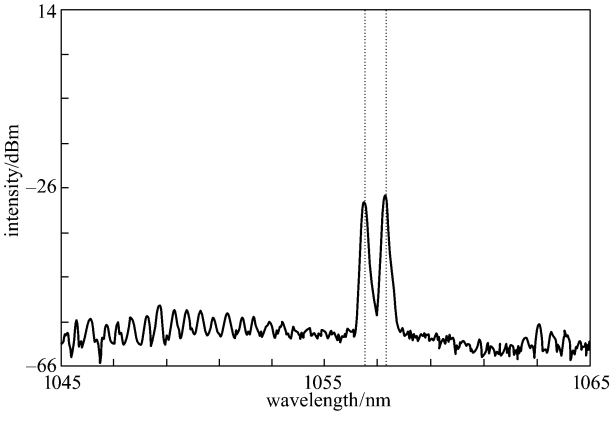

Fig. 15 Output spectrum of laser with FBG when screwed angle is 100°

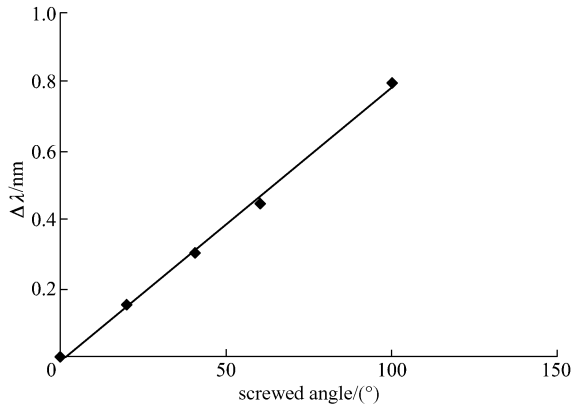

Fig. 16 Dependence of lasing wavelength spacing on screwed angle

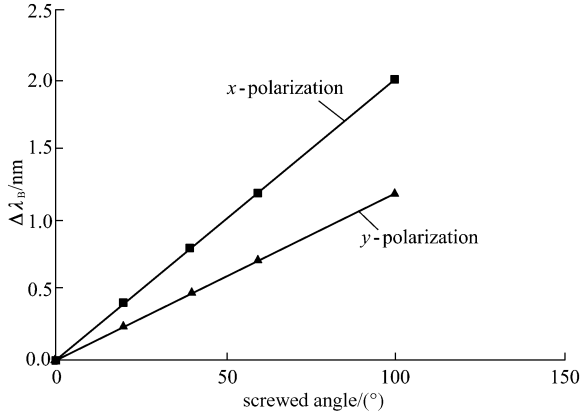

Fig. 17 Dependence of Bragg reflection wavelength variation on screwed angle for two polarized directions

4 Conclusions

In summary, the photosensitivity and the thermal decay of DCFBG are investigated, and the variation of amplitude of reflective-index modulation and effective reflective index with the UV exposure time are observed. Depending on the photosensitivity relations of all kinds of DCF, Bragg gratings of diversiform reflectivity with phase-mask method can be fabricated, and the maximum reflectivity of the grating is 99.9%. Using the experimental data obtained, we get the thermal decay characteristics according to the different annealing thermal properties, and these results are very significant to estimate the properties of grating. The resonant nonlinearity in an Yb^{3+}-doped DCFBG is studied by using pump laser wavelength of 976 nm, and the resonant nonlinearity in the DCFBG with central wavelength of 1056 nm is induced. The output spectrum of the grating with various incident power of pump lasers is recorded, and a strain-induced birefringence of rectangular inner cladding DCFBG is also presented. Through lateral strain applied on the grating, one reflection peak of the grating becomes two peaks. The wavelength spacing and the absolute wavelengths of the two polarizations of the grating can be tuned. Therefore, DCFBGs not only have potential applications in fiber communication and sensing, but also can be used in many other applications.

Acknowledgements This work was supported by the National Natural Science Foundation of China (Grant No. 60137010), the Hi-Tech Research and Development Program of China (Grant No. 2003AA312100), the Shandong Provincial Education Department Foundation of China (Grant No. J06P14) and the program of Qingdao Economic and Technology Development Area named “Research of FTTH and intelligent home commucation system based on POF link”.

References

1. Pask H M, Archambault J L, Hanna D C, et al. Operation of cladding-pumped Yb^{3+}-doped silica fiber lasers in 1μm region. Electronics Letters, 1994, 30(11): 863–865.
2. Yahel E, Hardy A. Efficiency optimization of high-power Er^{3+}-Yb^{3+}-codoped fiber amplifiers for wavelength-division-multiplexing applications. Journal of the Optical Society of America B, 2003, 20(6): 1189–1197
3. Ning D, Huang B C, Xiang Y, et al. Effect of back-cavity mirror on Yb^{3+}-double clad fiber. Acta Optica Sinica, 2003, 23(3): 313–316 (in Chinese)
4. Hill K O, Fuji Y, Johnson D C, et al. Photosensitivity in optical waveguide: Application to reflection filter fabrication. Applied Physics Letters, 1978, 32(10): 647–649
5. Hill K O, Malo B, Bilodeau F, et al. Bragg gratings fabricated in monomode photosensitive optical fiber by UV exposure through a phase mask. Applied Physics Letters, 1993, 62(10): 1035–1037
6. Chuang K P, Lai Y, Sheu L G. Complex fiber grating structures fabricated by sequential writing with polarization control. Optics Letters, 2004, 29(4): 340–342
7. Bilodeau F, Johnson D C, Malo B, et al. Ultraviolet-light photosensitivity in Er^{3+}-Ge-doped optical fiber. Optics Letters, 1990, 15(20): 1138–1140
8. Brambilla G, Pruneri V, Peekie L. Photorefractive index gratings in SnO2:SiO2 optical fibers. Applied Physics Letters, 2000, 76(7): 807–809
9. Pal S, Sun T, Grattan K T V, et al. Bragg gratings written in Sn-Er-Ge-codoped silica fiber: investigation of photosensitivity, thermal stability, and sensing potential. Journal of the Optical Society of America A, 2004, 21(8): 1503–1511
10. Oh S T, Han W T, Paek U C, et al. Discrimination of temper-ature and strain with a single FBG based on the birefringence effect. Optics Express, 2004, 12(4): 724–729
11. Archambault J L, Grubb S G. Fiber gratings in lasers and amplifiers. Journal of Lightwave Technology, 1997, 15: 1378–1390
12. Li L J, Fan W D, Wang Z, et al. Experimental studies on narrow-linewidth Yb^{3+}-doped double-clad fiber-laser cavities based on double-clad fiber Bragg gratings. Microwave and Optical Technology Letters, 2005, 44(1): 53–56
13. Li L J, Feng X H, Liu Y G, et al. Experimental investigation of high power Erbium-Ytterbium co-doped double clad fiber laser. Chinese Physics Letters, 2004, 21(12): 2426–2428
14. Li L J, Liu Y G, Jia X J, et al. Resonant nonlinearity in Ytterbium-doped double-clad fiber Bragg grating. Microwave and Optical Technology Letters, 2006, 48(3): 430–432

15. Li L J, Wang Z, Fan W D, et al. Yb^{3+}-doped double-clad fiber laser with all fiber cavity. Chinese Optics Letters, 2004, 2(10): 592–594
16. Li L J, Fan W D, Fu S G, et al. Yb^{3+}-doped double-clad fiber laser with frequency selecting by double-clad fiber Bragg grating. Acta Optica Sinica, 2005, 25(1): 55–58 (in Chinese)
17. Li L J, Wang Z, Fan W D, et al. Wavelength chirp-free tunalbe Yb^{3+}-doped double cladding fiber laser. Acta Photonica Sinica, 2005, 34(2): 184–186 (in Chinese)
18. Li L J, Sun L, Fan W D, et al. A strain-induced birefringent double-clad fiber Bragg grating. Chinese Optics Letters, 2005, 3(7): 383–385